Annals of Nuclear Energy 191 (2023) 109934

Contents lists available at ScienceDirect

Annals of Nuclear Energy

journal homepage: www.elsevier.com/locate/anucene

ALFRED reactor and hybrid systems: A test case

Riccardo Chebac [a,*], Antonio Cammi [a], Marco E. Ricotti [a], Stefano Lorenzi [a], Khashayar Sadeghi [b], Seyed Hadi Ghazaie [b], Ekaterina Sokolova [b], Evgeniy Fedorovich [b]

[a] Politecnico di Milano, Department of Energy, Nuclear Engineering Division, Via La Masa 34, 20156 Milan, Italy
[b] Peter the Great St. Petersburg Polytechnic University, 195251, Russian Federation

ARTICLE INFO

Keywords:
SMR
Hybrid systems
Cogeneration
Nuclear energy
Generation IV
Desalination

ABSTRACT

Future electricity generation will likely rely on renewable energy sources with consequent power intermittency and grid instability issues that will need to be compensated for. In this work, a model of a Generation IV small modular reactor has been developed in order to study its capabilities as a grid stabilizer. The plant model has been developed in Dymola and exported in the Simulink environment for the control strategy. The hybrid system considered couples a lead-cooled fast reactor to a desalination plant, an energy storage system, renewable energy farms, a variable electrical load, a local grid, and an external interconnected grid. Different desalination plants have been considered. Reverse osmosis has proven to be the most suitable option when coupled with energy production systems. Different configurations of the hybrid system have been considered showing a higher degree of load-following capabilities for the nuclear plant studied.

1. Introduction

It is widely anticipated that to reach the Paris Agreement's goal of maintaining the increase of the average Earth's temperature below the 2 °C mark by the end of this century, the energy produced by renewables will steadily increase to up to 45% of the total world electricity production by 2040 (Kober et al., 2020; Arroyo and Miguel, 2020). This approach will likely bring grid stability and availability issues (Yap et al., 2019; Ayamolowo et al., 2020), which in turn may lead to a strong dependence on storage systems and small flexible power plants for compensation. Given its low carbon footprint and dispatchability, nuclear power plants (NPP) could be an attractive solution to couple with renewable energy sources (Ingersoll et al., 2015; Suman, 2018). The NPP development in the last decades had a common trend, where increasing the reactor size seemed the most economical way to be competitive with fossil fuels. The economy of scale is ultimately what led to the NPP evolution e.g., from the Westinghouse AP600 to the AP1000. Other Generation III and III + reactors showed the same trend such as the Advanced Pressurized Water Reactor (APWR)-Mistubushi and the European Pressurized Reactor (EPR)-AREVA with a nominal electrical power of 1700MWe for the former and 1600MWe for the latter (Krautmann and Solow, 1988). Unfortunately, as stated by Locatelli et al. (Locatelli, 1802), the continuous delays and budget overruns during some large NPP construction projects makes the economies of scale potentially critical. The deployment of large NPPs involves a considerable economic-financial risk, which has been further exacerbated by the renewed attention to safety following the Fukushima accident. This, together with a widespread concern regarding environmental issues such as greenhouse gas emissions has renewed interest in Small Modular Reactors (SMR), technology which may mitigate some of these risks. Defined by the International Atomic Energy Agency (IAEA) as reactors with nominal power equal to or less than 300MWe (Subki, 2020), several SMR concepts promise to implement enhanced safety features, easy transportability and deployment, modularization, on-shop construction, and lower financial risk. Historically NPPs have been deployed for the production of baseload electricity. Some countries such as France and Germany have successfully used their NPPs also in load follow mode (Lokhov, 2011), varying the power generation by means of control rod adjustment in Pressurized Water Reactors (PWR) and by changing the coolant flow rate in Boiling Water Reactors (BWR). The control strategies mentioned aim at varying the reactivity of the fission reaction, thus the nominal power output, which can introduce thermomechanical stresses in the primary loop if not properly managed. According to a report by the Organization for Economic Cooperation and Development – Nuclear Energy Agency (OECD-NEA) (OECD Nuclear Energy Agency, 2021), there are certain operating modes that do not reduce the fatigue strength of equipment in nuclear power plants.

* Corresponding author.
E-mail address: Riccardo.Chebac@polimi.it (R. Chebac).

https://doi.org/10.1016/j.anucene.2023.109934
Received 31 January 2023; Received in revised form 11 May 2023; Accepted 17 May 2023

These modes include operating within a frequency regulation range of ± 5% rated power (Pr) with ramps of 1% the Pr per second, reactor power level variations of less than 5% Pr per minute and magnitude of less than 10% Pr and changing the reactor power by ± 10% Pr with the speed of 5% Pr per second. There are also limitations on the total number of cycles for certain operating modes. Load following with a speed of less than 5% Pr per minute in the power range of 50% Pr to 100% Pr is limited to 20,000 cycles while changing the reactor power by ± 20% Pr with the speed of 10% Pr per minute is limited to 20,000 cycles. A second problem refers to the primary frequency stabilization of the grid which leads to possible loss of revenues if the grid stabilization is not adequately remunerated. Locatelli et al. (Locatelli et al., 2017) have reported that operating a nuclear reactor at a power level 2–3% lower than nominal will increase the levelized cost of electricity (LCOE). However, as shown in (OECD Nuclear Energy Agency, 2021) the lowering of the capacity factor together with the current discount rates is not enough to jeopardize the competitiveness of nuclear power. An average capacity factor of 65% or lower with a discount rate of 5% or higher is required to reduce the competitive advantage of NPPs. Nonetheless, an increase in competitiveness can be offered by a "load following by cogeneration" approach (Locatelli et al., 2017) where the thermal power is kept stable at nominal capacity, during the high load/high price hours of the day and during low demand/low price periods, the excess power will be redirected to external, cogeneration systems such as desalination plants, biofuel or hydrogen production facilities, and district heating. A fleet of SMRs can be an particularly attractive for cogeneration purposes compared to conventional large reactors due to their intrinsic modularity, allowing for flexibility in power output management by diverting heat from some units while keeping others at full power. It is crucial to clearly define the hybrid system being considered. For example, different thermal desalination processes require different heat fluxes with temperatures ranging from 65 to 150 °C (International Atomic Energy Agency, 2017). Different types of reactors are suitable for different types of cogeneration. As illustrated in Fig. 1, LWRs have limited applicability for load following by cogeneration, whereas generation 4 (Gen IV) reactors offer greater versatility (Lee et al., 2009; Zohuri, 2020; Jerome Serp et al., 2014). However, some of the limitations of LWRs may be overcome by employing heat augmentation techniques. For instance, the Idaho National Laboratories (INL) has been studying these techniques for high-temperature steam electrolysis, as reported in (You et al., 2017). Investigating optimal coupling options between reactor technologies and industrial processes can reveal potential synergies that can enhance the integration of renewable energy sources into the grid. An example is provided in Fig. 2. The IAEA already carried out studies regarding the economic potential of hybrid systems in different scenarios (Nuclear–renewable hybrid energy systems for decarbonized energy production and cogeneration, xxxx) showing higher profitability when nuclear is coupled with low capital cost industrial processes. To guage the different possible combination of system coupling, the following paper will present a preliminary study on a novel hybrid system simulator developed that can evaluate the technical feasibility over a 24-hour period of various hybrid system scenarios in the current energy landscape. The object-oriented and modular design of the simulator enables easy modification and fast simulation run times by simply dragging and dropping sub-models. The study will be carried out on a model of the Advanced Lead-cooled Fast Reactor European Demonstrator (ALFRED) (Alessandro Alemberti, et al., 2013), modified for steam extraction for heat application processes. It will examine the potential for load following via cogeneration in a grid with 10 MWe of photovoltaic (PV) and a 10 MWe wind farm. The NPP will be run in both load following and baseload configurations. Different electrical systems such as battery storage and reverse osmosis (RO) will be evaluated and compared as thermal desalination methods. The paper is organized as follows: Section 2 provides an overview of the MODELICA model and simulator. Section 3 describes the general Simulink blocks, focusing on the NPP controller, renewable

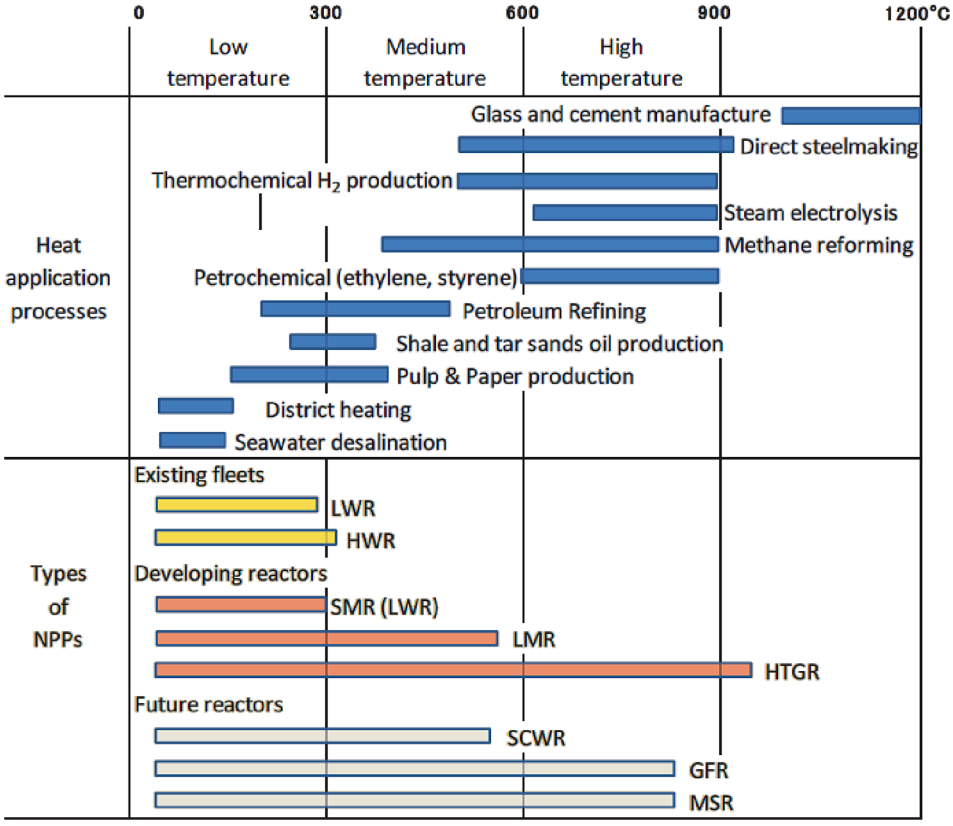

Fig. 1. Temperature ranges of heat application processes and types of nuclear power plant (Opportunities for Cogeneration with Nuclear Energy, 2017).

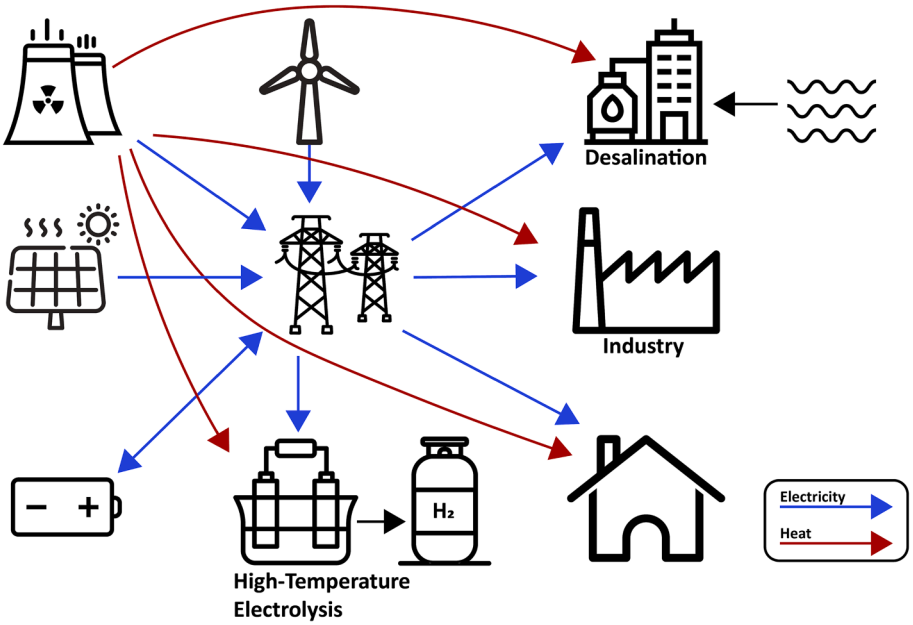

Fig. 2. Example of hybrid system configuration, implementing SMR units, cogeneration plants, variable renewables, and energy storage into a local grid.

and energy storage systems, and thermal and electric desalination blocks. Section 4 presents the results from analyzing various configurations in selected case studies. Lastly, Section 5 offers a summary and conclusion of the work.

2. Model based on MODELICA

Previous studies have developed NPP simulators using various platforms, including Matlab/Simulink (Dong and Pan, 2018; Dong et al., 2018; Dong et al., 2019), in-house codes based on Matlab (Son et al., 2021), and professional software such as Ebsilon (Wang et al., 2021). However, the use of Matlab platform may become cumbersome for detailed and complex plant models, as it is more suitable for dynamic analysis of lumped parameter systems. In contrast, previous studies conducted by the Department of Energy (DOE) under the Integrated Energy Systems (IES) program (Frick et al., 2019) have demonstrated the capabilities of an acausal language, such as MODELICA (Dizqah et al., 2013; Elmqvist et al., 1998), in evaluating the techno-economic feasibility of complex systems, such as hydrogen production using Light Water Reactors (LWRs). The flexibility and modularity of MODELICA have been further confirmed by the addition of thermal distribution systems to the model (Frick et al., 2020; Mikkelson et al., 2021) in subsequent instances. Based on these considerations, an object-oriented approach is implemented using Dymola (Dag Brück et al., 1996; Otter et al., 1996) software, which utilizes the MODELICA language. This modeling method offers several advantages over the commonly used causal approach for simulating physical systems, including:

1. Flexibility and modularity: The object-oriented approach allows for modular and flexible modeling of complex systems, making it easier to incorporate new components or subsystems into the model.
2. Reusability: The use of object-oriented programming principles allows for the creation of reusable components, which can be easily modified or extended for different applications or scenarios.
3. Causality independence: The acausal nature of MODELICA allows for modeling of systems without explicitly defining the causal relationships between components, making it more suitable for modeling multi-physics or multi-domain systems.
4. System-level analysis: The object-oriented approach enables system-level analysis, where the interactions between different components or subsystems can be easily captured, leading to a more comprehensive understanding of the overall system behavior.

Overall, the utilization of an object-oriented approach with the Dymola software and the MODEL- ICA language provides a robust and flexible framework for simulating complex nuclear energy systems, allowing for detailed and accurate analysis of their dynamic behavior and techno-economic feasibility. The resulting software offers a multi-engineering approach, leveraging the extensive selection of libraries available for MODELICA, which enable multi-field modeling of complex integrated engineering systems with fast simulation run times. Additionally, the symbolic manipulation capabilities of the software make it intuitive to model with. These qualities are critical for the goal of this work, which is to develop a highly modular simulator that can be easily adapted for different cases. The ALFRED NPP model is based on the simulator created by Ponciroli et al. (Ponciroli et al., 2014). The use of an object-oriented approach and the availability of various open libraries enable a versatile and efficient simulation framework for complex integrated engineering systems. This allows for rapid development and customization of simulation models, making it adaptable to different scenarios and applications. The simulator's modular nature facilitates easy incorporation of specific components or subsystems, making it a powerful tool for studying the ALFRED power plant or other similar systems.

2.1. Reactor core and primary loop models

The core has been developed within the Dymola environment by implementing point reactor kinetics (Oka and Suzuki, 2013; Akcasuh, 2012) (Eq.1) with eight delayed neutron precursor (c_i) groups to describe neutron density (n) evolution and 1-D heat transfer model. The heat exchange between fuel and coolant is calculated using the Ibragimov-Subbotin-Ushakov correlation (Kh Ibragimov et al., 1961; Agosti, et al., 2007).

$$\begin{cases} \dfrac{dn}{dt} = \dfrac{\rho_{reac} - \beta}{\Lambda} n + \sum_{i=1}^{8} \lambda_i c_i + S \\ \dfrac{dc}{dt} = \dfrac{\beta_i}{\Lambda} n - \lambda_i c_i \qquad i = 1 \div 8 \end{cases} \tag{1}$$

With S being the source term expressed in neutrons/s, ρ_{reac} the

reactivity expressed in PCM, β the fraction of the neutrons that appear as delayed neutrons in the i-th group, Λ the prompt neutron generation time expressed in seconds, and λ the decay constant for the i-th group expressed as $1/s$. As shown in Fig. 3, the core block is divided into three sub-blocks. The kinetics block describes both the neutrons and precursor density evolution. Two effective fuel temperatures have been implemented to model the fuel pellet, namely:

$$T_f^D = 0.3T_f + 0.7T_f^3 \tag{2}$$

$$T_f^{eff} = 0.5T_f + 0.5T_f^3 \tag{3}$$

where $T_f{}^D$ is the fuel temperature describing the Doppler effect and $T_f{}^D$ represents the effective fuel

temperature describing the reactivity feedback given by thermal stresses which deform the pellet. The reactivity variation due to the Doppler effect can be considered via the following equation:

$$\Delta\rho\left[T_{f1}\rightarrow T_{f2}\right] \approx 1.1K_D\left(\frac{T_{f2}^D}{T_{f1}^D}\right) \tag{4}$$

where KD is the Doppler constant expressed in pcm. The reactivity variation given by coolant density, and axial and radial cladding expansions have been considered via linear equations with constant coefficients. Moreover, a negative feedback coefficient is considered for the core volume expansion which in turn produces increased neutron leakages. For the control rods, a reactivity differential curve has been adopted considering the reactivity worth of 12 rods at different insertion lengths. A lower degree of accuracy has been given for the safety rods since they were extracted at start- up. Therefore, the total reactivity of the system can be calculated as seen in equation (5). Where the 13 terms are in order the initial reactivity margin, the effect due to lead density, Doppler effect, axial cladding expansion, radial wrapper expansion, axial fuel expansion, diagrid expansion, pad effect, control rod contribution, and safety control rod distribution and the various α being the feedback coefficients for every component.

$$\begin{aligned}\rho(t) = \quad & \rho_0 + \alpha_L\left(T_l - T_{l,0}\right) + 1.1{\cdot}K_D\left(\frac{T_{f2}^D}{T_{f1}^D}\right) + \alpha_{CZ}\left(T_c - T_{c,0}\right) \\ & + \alpha_{WZ}\left(T_l - T_{l,0}\right) + \alpha_{CR}\left(T_c - T_{c,0}\right) + \alpha_{WR}\left(T_l - T_{l,0}\right) + \alpha_{FZ}\left(T_c - T_{c,0}\right) \\ & + \alpha_{Dia}\left(T_{l,\ \text{in}} - T_{l,\ \text{in},0}\right) + \alpha_{\text{Pad}}\left(T_{l,\ \text{out}} - T_{l,\ \text{out},0}\right) \\ & + A_{CR}{\cdot}sin(B_{CR}{\cdot}h_{CR} + C_{CR}) + D_{CR} + A_{SR}{\cdot}\frac{(h_{SR} - x_{SR})}{LSR}\end{aligned} \tag{5}$$

The thermal behavior of the fuel pins is modeled via the Fuel Rods block by implementing a time- dependent Fourier equation. The fuel pin is discretized in five radial zones, three for the fuel pellet, one for the helium gap, and one for the cladding. The fuel equation is the following:

$$\rho_f c_f \frac{\partial T_f}{\partial t} = \frac{1}{r}\frac{\partial}{\partial r}\left(rk_f\frac{\partial T_f}{\partial r}\right) + q''' \tag{6}$$

For the Helium gap, a steady-state condition has been considered:

$$\frac{1}{r}\frac{\partial}{\partial r}\left(rk_g\frac{\partial T_g}{\partial r}\right) = 0 \tag{7}$$

Finally, the time-dependent equation governing the cladding behavior reads:

$$\rho_c c_c \frac{\partial T_c}{\partial t} = \frac{1}{r}\frac{\partial}{\partial r}\left(rk_c\frac{\partial T_c}{\partial r}\right) \tag{8}$$

Longitudinally the equations can be discretized by a user-defined value. The third component, Lead Tube, models the single-phase liquid flow of molten lead through cylindrical pipes with heat transfer from the fuel pin boundary. The physical properties of the fluid are all considered temperature- dependent. To describe the dynamics of pressure and mass flow rate of the system, the mass balance Eq.9, and momentum balance Eq.10 equations have been adopted.

$$A\frac{\partial \rho}{\partial t} + \frac{\partial \Gamma}{\partial x} = 0 \tag{9}$$

$$\frac{\partial \Gamma}{\partial t} + A\frac{\partial p}{\partial x} + A\rho g\frac{\partial z}{\partial x} + \frac{C_f\omega}{2\rho A^2}\Gamma|\Gamma| = 0 \tag{10}$$

2.2. Steam generator model

A simplified one-dimensional steam generator (SG) model, as shown in Fig. 4, is adopted. The model incorporates a counter-current configuration. For the Water Side, the Dittus-Boelter correlation for single-phase heat transfer and the Chen correlation from the MODELICA library Thermo Power (Casella and Leva, 2005) for two-phase heat transfer are applied. The Ibragimov-Subbotin-Ushakov correlation for single-phase liquid metal heat transfer is used for the Lead Side as well (Kh Ibragimov et al., 1961). The SG block represents the combined effect of eight bayonet-type SGs, equivalent to the number in the ALFRED

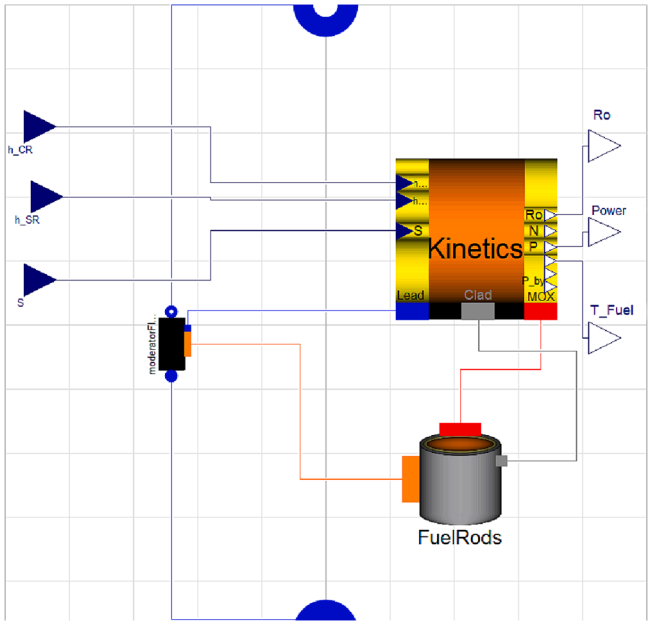

Fig. 3. Dymola reactor core and primary loop model.

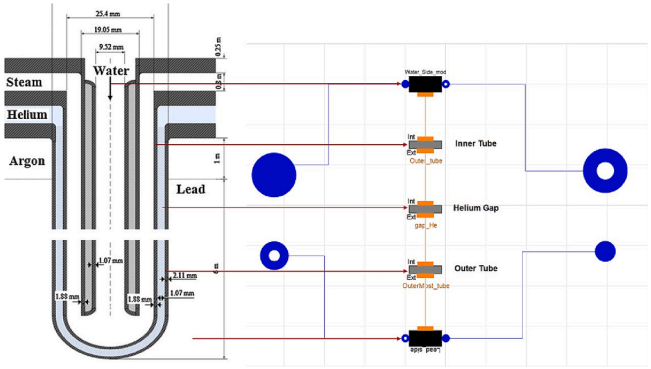

Fig. 4. Bayonet type SG: scheme with MODELICA representation.

nuclear power plant, which is modeled as one SG with a power of 300 MWth. The nominal parameters of this technology are summarized in Table 1. To enhance the description of heat transfer within the SG, different wall interfaces are modeled using conductive elements. Thermal resistances are computed using the Fourier equation, allowing for the evaluation of the impact of the inner and outermost tube, as well as the helium gap, on the overall thermal performance of the system.

2.3. Turbine

The Steam turbine unit is employed to simulate a high and low-pressure stage using the Thermo Power library. The turbine group is divided into two sections, an upper and a lower pressure stage, to deliver a maximum power of 130 MWe under nominal conditions, as shown in Fig. 5. The model is also flexible in terms of selecting the desired pressure of the extracted steam to study different cogeneration scenarios. In our case, the extraction pressure is set to 0.5 bar, enabling the extraction of saturated steam at approximately 80 °C, suitable for a multi-effect distillation (MED) desalination plant. Table 2 provides the main design parameters for the turbine group. The results of tests on control rod insertion and withdrawal, ramping up the water mass flow rate in the secondary loop, and extraction valve characterization are consistent with the design parameters and characteristic times of the envisioned plant as shown in the previous study (Chebac et al., 2021). The admission valve shown in Fig. 5 can be used to control the mass flow rate entering the turbine. At the inlet, the steam is superheated, hence the relationship between the mass flow rate (Γ) and pressure (P) at the inlet is approximately proportional to the admission valve opening coefficient (k_v) as expressed in Eq.11.

$$\Gamma \approx k_v P \tag{11}$$

3. Matlab Simulink

In the following section, the Simulink libraries and controller model will be presented in detail. Simulink is chosen for its seamless interoperability with the Dymola environment, user-friendly interface, and extensive collection of pre-built blocks and functions that facilitate the construction of complex systems. This choice enables a robust and efficient implementation of the controller model, leveraging the capabilities of both Dymola and Simulink for a comprehensive analysis of the system dynamics and control performance.

3.1. Reactor controller

A reactor controller is developed to maintain nominal plant parameters, enable steam extraction for cogeneration, and perform primary frequency regulation. Given the slow flow speed and large thermal inertia of lead as a coolant, varying the core thermal output as is done in LWRs would be ineffective for load-following purposes. Therefore, the control strategy developed by Ponciroli et al. (Ponciroli et al., 2015) is adopted, which decouples the primary loop from the balance of plant and works solely on the steam entering the turbine by venting the excess steam directly to the condenser. Additionally, to avoid thermal and mechanical stresses on the SG, a constant pressure operation mode on the turbine inlet is chosen. Furthermore, it is essential to maintain the lead's lowest temperature at a value of 400 °C or higher to avoid possible freezing of the coolant and embrittlement of the components. An additional controller is added to enable steam extraction at the inlet of the low-pressure stage. This controller regulates the opening of two valves, the extraction valve, and the low-pressure valve, to enable steam extraction for the required cogeneration power. The controller is created in the Simulink environment with the imported MODELICA model, with aid from libraries such as Simscape Power Systems for the three-phase grid simulation environment. A detailed description of the controller can be found in Appendix A.

Table 1
Single bayonet SG parameters.

Parameter	Value	Units
Thermal power	37.5	MW_{th}
Feedwater inlet temperature	335	∘ °C
Feedwater outlet temperature	450	°C
Steam pressure	180	bar
Length of heat exchange	6	m
Number of tubes	510	–

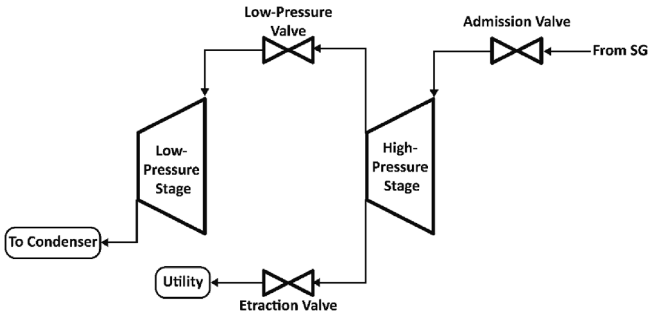

Fig. 5. MODELICA turbine group schematic.

Table 2
Turbine main design parameters.

Parameter	Value	Units
Mechanical power	130	Mw
Inlet temperature	450	°C
Inlet pressure	180	bar
Extraction temperature	80	°C
Extraction pressure	0.5	bar
Nominal mass flow rate	192	kg/s

3.2. Renewables and storage

The models for battery storage, solar panels, and wind turbines are carefully selected from a verified library developed by MathWorks (Jonathan LeSage, xxxx) and are adapted to operate in a 50 Hz grid. The unique advantage of this library is the simplicity of the blocks, which directly interface with a three-phase grid without the need for additional inverters, buck-boost converters, or other complex components. The Solar Farm block, for example, takes solar irradiance (W/m^2) as input and can be easily customized by adjusting the efficiency of the panels and the total area covered by the farm. The parameters are chosen to achieve a theoretical maximum electricity production of 10 MWe for the solar farm, with the model accurately calculating the power output of the panels using a simple equation that considers efficiency, irradiance, and total area of the plant, as shown in Eq.12.

$$P = \eta_{panel} A_{plant} Irr \tag{12}$$

Where Irr is the solar irradiance in W/m^2, η_{panel} is the efficiency of the panel assumed to be 10%, and A_{plant} is the total area of the solar farm considered to be 1000 m^2. The calculated power is then appropriately converted to the specific voltage and current requirements of a three-phase configuration, ensuring the representation of the solar panel's performance in the system.

The Wind Farm block requires wind speed as input and needs the nominal power, nominal wind speed, and maximal or cut-off wind speed to be specified. The parameters in Table 3 are chosen to take into account a value slightly higher than the average wind speed in Milan (2–3 m/s (Weatherspark, xxxx). The model is divided into two blocks: controller and power production. The power is calculated as in Eq.13, considering it to be proportional to the cube of the wind speed.

Table 3
Wind farm model parameters.

Nominal power (MWe)	Nominal wind speed (m/s)	Maximal wind speed (m/s)
10	5	15

$$P_{WT} = \frac{1}{2} C_P \rho_{air} A_{rotor} v^3 \quad (13)$$

where C_P is the power coefficient (usually measuring between 0.3 ÷ 0.4). The maximum theoretical power obtainable by this coefficient is $C_{P\_max} = 0.59$, known as the Betz Limit (Ragheb and Ragheb, 2011). The power coefficient is kept constant. A Boolean controller is used which disconnects the turbine in case the wind speed reaches the cut-off value. In Fig. 6 the input data for solar irradiance and wind speed are provided.

Finally, the Energy Storage model is designed to represent the behavior of the battery storage, considering grid frequency, voltage, capacity, power, and charge/discharge controls. This block incorporates an under/overcharge controller that constantly monitors the state of charge (SOC) of the system. If the SOC exceeds a predetermined threshold, the power entering/exiting the battery will be interrupted to prevent overcharging or over-discharging. Additionally, an SOC calculator is included in the model, which considers the capacity and power of the system to accurately estimate the current SOC. The nominal power output of the battery storage system is set to 5 MWe, and the calculated power required or delivered by the system is then transmitted to a three-phase dynamic load block. This block converts the input power into a three-phase signal that can be seamlessly integrated with the rest of the grid, ensuring representation of the energy storage system's behavior in the overall system simulation.

3.3. Desalination

The use of cogeneration for desalination plants is the focus of the case study presented. The increasing challenges related to freshwater shortages worldwide highlight the need for new technologies and methods that can improve efficiency and reduce carbon emissions. One practical solution is the use of seawater desalination technology in arid and semi-arid regions (Ghazaie et al., 2019), where freshwater consumption often exceeds its reproduction rate. However, a major drawback is the high energy consumption and associated cost of desalination processes, with 47% of operating costs being attributed to electricity and thermal energy costs (Al-Karaghouli and Kazmerski, 2013). The energy required to produce one cubic meter of freshwater varies between 2.5 kWh and 8.5 kWh (Ghazaie et al., 2020) depending on the technology (Youssef et al., 2014), making freshwater production costly. Additionally, the environmental impact of seawater pumping, and concentrated brine discharge must also be considered. In recent years, researchers have developed more affordable desalination technologies (Kavvadias and Khamis, 2010) to address the saline water issue. The main commercial technologies employed in large-scale systems are based on two processes: evaporation/condensation (thermal method) and membrane. Thermal desalination technology can be broadly classified into two groups: multi-stage flashing (MSF) and MED. Both methods require heat and electrical energy and can treat high salt-concentration water (70 g/L). Among all the membrane techniques, RO is considered the leading pressure-driven membrane process and is widely used in large-scale desalination plants. Currently, more than 60% of overall freshwater production worldwide is produced by this technology given its low cost and high reliability compared to other thermal desalination methods. RO desalination plants rely solely on electrical energy, unlike thermal desalination methods. Current research in the desalination field aims to reduce the overall cost of water production and enhance the efficiency of cogeneration plants (Sadeghi et al., 2020). The main parameters of RO and MED are provided in Table 4 with and a detailed overview of the desalination models developed is given in Appendix B.

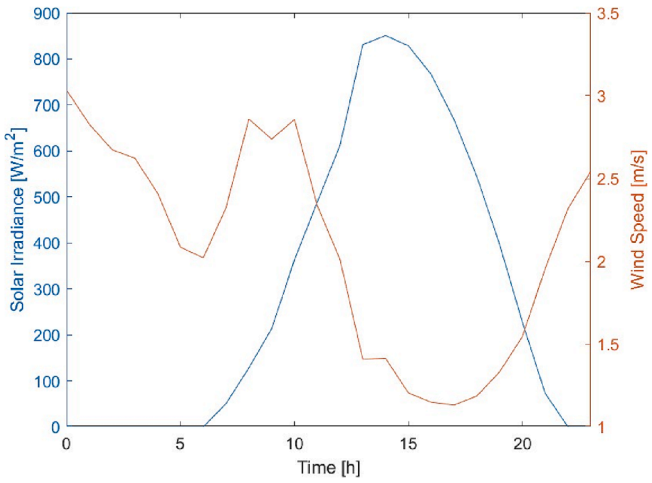

Fig. 6. Input data of solar irradiance and wind speed for the 13th of July 2020.

4. Case studies and results discussion

In order to investigate the grid response and stress imparted to a hybrid system that incorporates nuclear and renewable energy sources, a European test bench has been selected. The Milano area grid is chosen, along with corresponding energy demand and meteorological data. Three hybrid system (HS) configurations are considered: HS0 (reference case), HS1 (electricity-based cogeneration and storage), and HS2 (thermal-based cogeneration, no storage). Four case studies are analyzed: one each for the HS0 and HS2 scenarios, and two cases for HS1 by assuming different seasonal loads (summer and winter). The hybrid system configurations are summarized in Table 5. To simplify the calculation, a downshift of the higher daily summer load curve is assumed to simulate the winter load, by considering a baseload value of 83 MWe (winter) instead of 98 MWe (summer), with the daily variable load being between 24.7 MWe and 46.9 MWe for both seasons. For the purely electrical systems (HS1), a pre-programmed charge/discharge battery control strategy is adopted, with the excess electrical production being redirected to the RO plant. For thermal cogeneration (HS2), a pre-programmed thermal load during the night hours is used for a MED desalination plant. This option serves as a simplified proof of concept for a possible cogeneration control strategy. The case studies aim to demonstrate the feasibility of integrating a Gen IV SMR into the hybrid system by limiting thermomechanical stresses and thermal gradients on the plant. Additionally, it is of particular interest to analyze which solution will offer less solicitation to the external, interconnected grid for both primary frequency stabilization and load following. Fig. 7 represents the coupled MODELICA plus Simulink dynamic simulator, while Fig. 8 shows the schemes of the two configurations of the hybrid systems, adopted for HS1 and HS2 case studies. The grid consists of a 220 kV and a 20 kV section. The reactor is considered to be distant 20 km from the medium tension utility while the rest of the grid is connected via an 80 km line. The value of the network's resistance over reactance

Table 4
Operational and performance parameters of RO and MED desalination technologies (New Technologies for Seawater Desalination Using Nuclear Energy, 2015).

Parameters	MED	RO
Operating temperature (°C)	65–70	Ambient
Thermal energy (kWh/m^3)	40–65	–
Electric energy (kWh/m^3)	2.0–2.5	4.0–6.0
CO_2 emissions (kg/m^3)	7.0–17.6	1.7–2.8
Tons f water required per ton of water production	5–8	2–4

Table 5
Summary of the different components considered in the various case studies (*covered by GenIV SMR).

Case Study	Load min–max	(Baseload) *	GEN IV-SMR	PV
	MWe	MWe	MWe	10 MWe
HS0	122.7–144.9	(98)	130 - Full load	✓
HS1 (summer)	122.7–144.9	(98)	130 - Full load	✓
HS1 (winter)	107.7–129.9	(83)	130 - Load follow	✓
HS2	122.7–144.9	(98)	127 - Progr. load	✓
	Wind	Batteries	RO	MED
	10 MWe	5 MWe		15 MWth + 7 MWe
HS0	✓	–	–	–
HS1 (summer)	✓	✓	✓	–
HS1 (winter)	✓	✓	–	–
HS2	✓	–	–	✓

ratio has been set to 7 which is typical of a 220 kV transmission line (Dimensioning of current transformers for protection applications, xxxx). The network is considered fully meshed with a 2 GWe power production system, which can compensate for power imbalances. The SMR operates in full load both in the reference scenario (HS0) and in the electrical-only scenario (HS1) in the summer, while it is in the load follow mode in the winter. In the thermal cogeneration scenario (HS2), a simple pre-programmed load has been adopted, to feed the MED plant during the night hours. As for the blocks pertaining to solar and wind farms, the inputs that have been used are the data relative to the 13th of July 2020 for energy demand, solar irradiance, and wind speed taken on an hourly basis. A Variable Load block has been added to account for the daily load variation.

4.1. Reference case HS0 – Gen IV SMR (full load) and renewables

The reference case scenario simulates the operation of a reactor working at full capacity in conjunction with renewable energy systems alone, lacking both energy storage and cogeneration capabilities. As a result, this configuration places the greatest demands on the grid. The daily total power produced by the hybrid system, in comparison to the load to be matched, is illustrated in Fig. 9. When the electricity demand (Load curve) exceeds the electricity production (HS curve), it signifies a surplus power production that needs to be supplied to the external grid, whereas when the HS curve is higher than the Load curve, additional power is required from the external grid. The primary objective of the HS1 and HS2 scenarios is to reduce these areas by incorporating load following, energy storage, or cogeneration systems, and to assess the viability of each configuration.

4.2. Case study HS1 (summer) – Gen IV SMR (full load), renewables, battery storage, and RO

As for the battery energy storage system is concerned, a pre-programmed time-controlled charge/discharge method has been assumed: during nighttime the batteries get charged, and during the day they are discharged (Charge/discharge control of battery energy storage system for peak shaving yahia baghzouz, xxxx). Fig. 10 shows the contributions from each power plant. The battery storage system is set to discharge condition after the point where the load curve becomes greater than the ALFRED power plant production. Of course, the time when this will happen can't be known in advance, but it can be approximated with good precision by looking at the data from the day before. The results of the energy demand, depicted in Fig. 11, reveal a significant improvement when compared to the reference case without battery storage, as shown in Fig. 9. The implementation of the energy storage system, using a basic control method, effectively minimizes the discrepancy between energy demand and supply. The load-following capabilities of the system can be further improved by redirecting the remaining electrical surplus to a RO desalination plant. This approach allows for the absorption of excess power production during low-

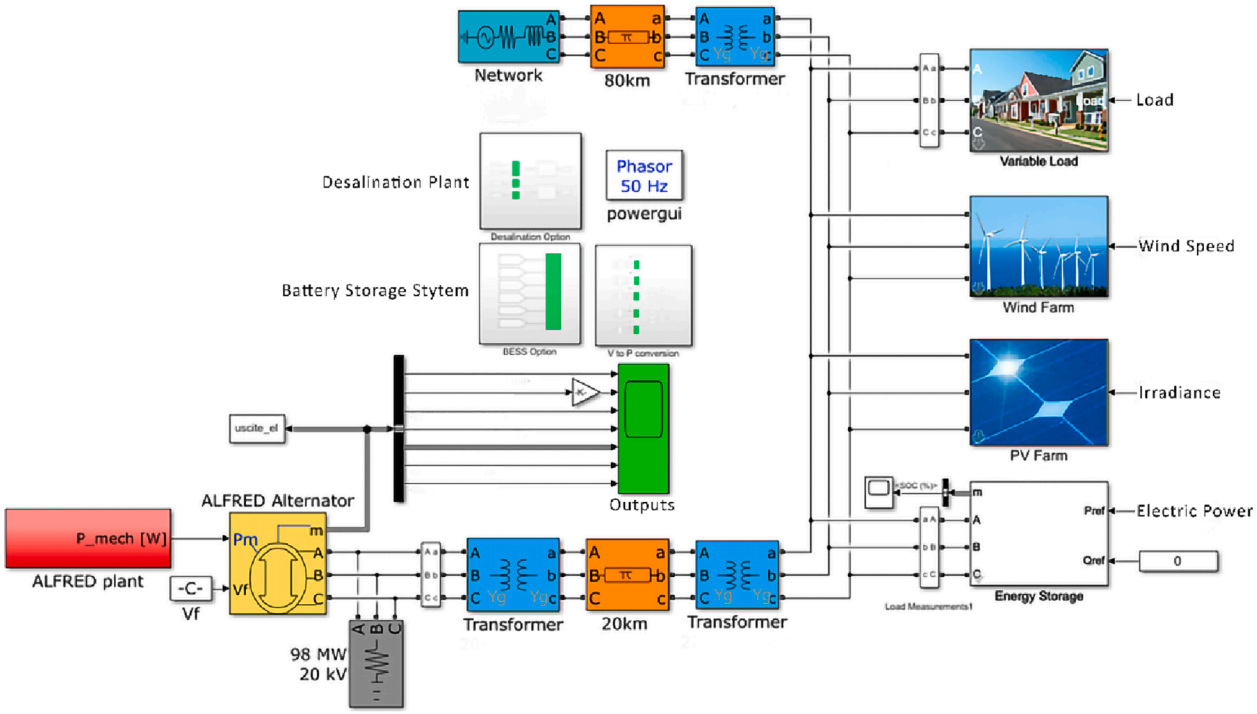

Fig. 7. Grid and plants Simulink model of the hybrid system for electrical loads only (HS1).

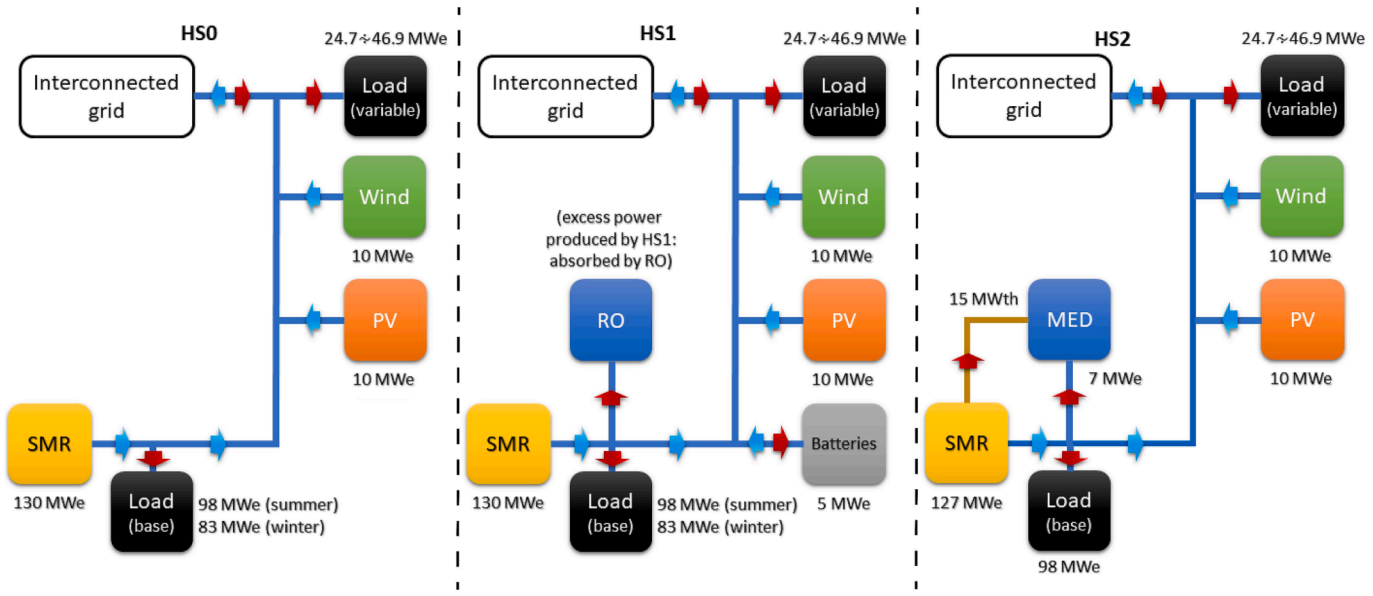

Fig. 8. Scheme of simulators for HS0, HS1, and HS2 scenarios.

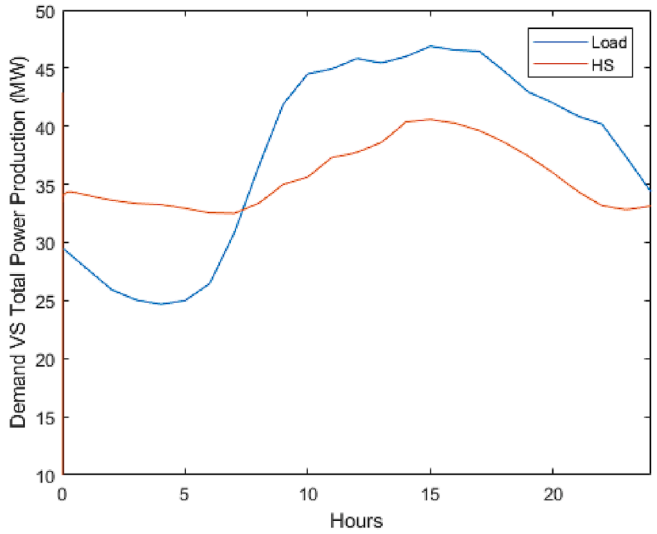

Fig. 9. Reference case HS0: Electrical demand VS. Total power produced.

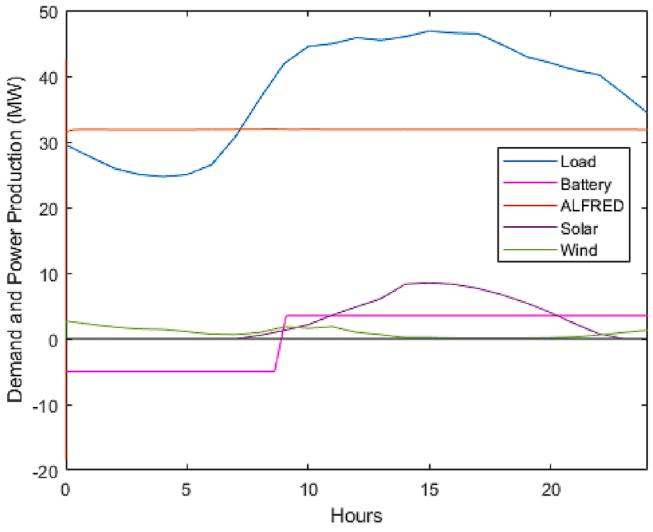

Fig. 10. HS1 (summer): Electrical demand and contributions for each power plant.

demand hours, reducing the stress on the grid. This is evident in the green area of Fig. 11, which represents the power absorbed by the RO plant. However, during high-demand hours, when electricity consumption exceeds power generation, the gap between load and power generated remains, as indicated by the red area in the same figure. The capacity of the RO desalination plant is illustrated in Fig. 12 where the values shown are in first approximation directly proportional to the power diverted to the RO plant as explained in detail in Appendix B.

4.3. Case study HS1 (winter): Gen IV SMR (load following), renewables and battery storage

This case study demonstrates the effectiveness of the hybrid system and the load-following controller in aligning with the electrical demand by dynamically adjusting the power output of the reactor and utilizing the energy stored in the battery system. To simulate a winter load scenario, the base load is lowered from 98 MWe to 83 MWe, and the variable loads in both summer and winter seasons, along with the power production capabilities of the hybrid system, are depicted in Fig. 13. A controller is employed to connect the grid load and frequency variations to the turbine admission valve to achieve load following and frequency stabilization in the summer season. The pressure and temperature controller in the plant secondary loop works in coordination with the frequency controller to maintain nominal values of the plant. The battery energy storage system is integrated with a pre-programmed charge/discharge strategy, resulting in battery power depletion around 17:00 and recharging starting at 22:00 (Fig. 14). The load is well-matched, as evident from the sum of all power contributions in Fig. 15. The abrupt cutoff of the battery at 17:00 (Fig. 16) causes a minor disruption in the grid, which is suitably managed by the plant, as depicted in Fig. 16, with the frequency remaining within safety margins. Although the reactor handles the rapid transients, as observed in Fig. 17 with minimal stress on the secondary side pressure, relying solely on the reactor for managing such fast changes in grid frequency may result in higher operation and maintenance (O&M) costs over time, and thus may not be optimal.

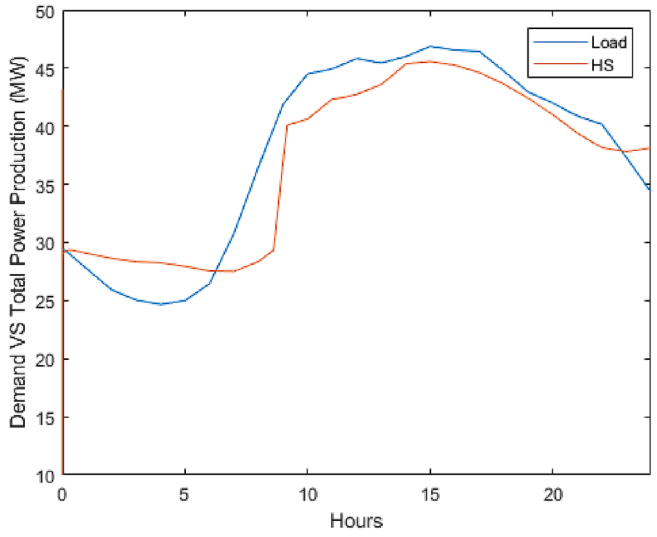

Fig. 11. HS1 (summer): Electrical demand VS. Total power produced (green: excess energy production - absorbed by RO plant).

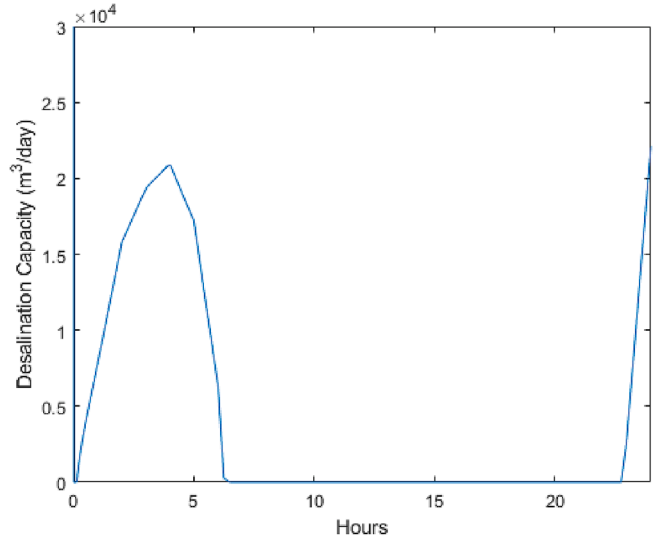

Fig. 12. HS1 (summer): Capacity of the RO plant during the day.

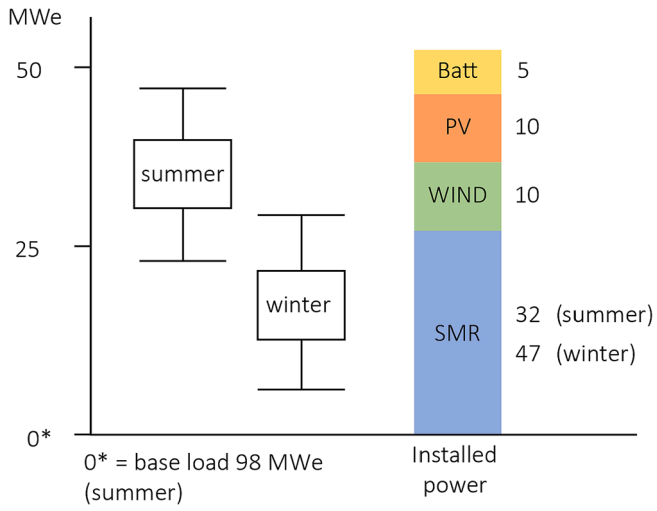

Fig. 13. Power capacity compared to the two seasonal load scenarios.

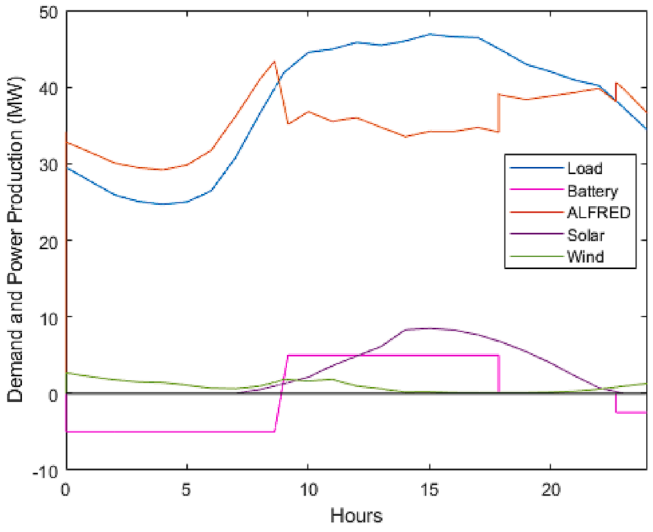

Fig. 14. HS1 (winter): Electrical demand and contributions.

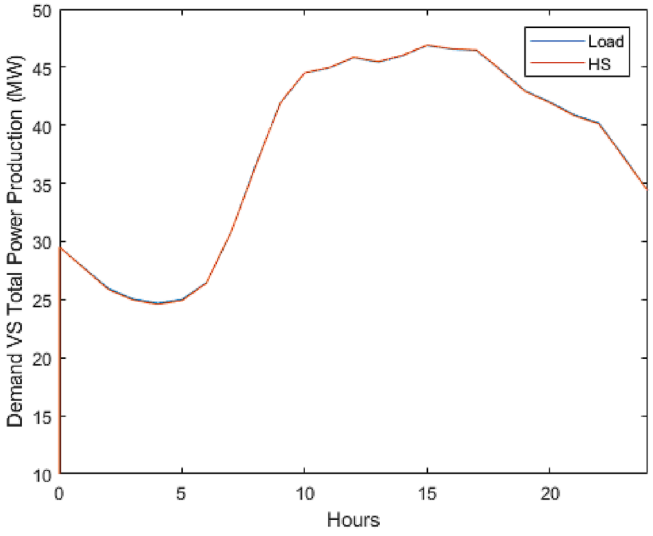

Fig. 15. HS1 (winter): Electrical demand VS. Total power produced (perfect load matching).

4.4. Case study HS2 – Gen IV-SMR (full load), renewables and MED

The final case study examines a thermal cogeneration scenario, in which the SMR supplies 15 MWth and 7 MWe of energy to a MED desalination (Fig. 20), according to a pre-programmed load-following strategy (Ayamolowo et al., 2020). This strategy is similar to the one adopted for the simulation of battery storage. The use of steam from the SMR balance of plant results in an efficiency reduction for the SMR thermal cycle, which is able to provide 127 MWe instead of 130 MWe when the MED is in operation. The 3 MWe SMR gap during the cogeneration mode is illustrated in Fig. 18, which shows all the electrical power contributions. The results in Fig. 19 demonstrate the matching capability of the hybrid system. In contrast to the HS0 and HS1 scenarios, a significant lack of power production also occurs during the night hours, when the MED plant absorbs both thermal and electrical power from the SMR to cogenerate desalinated water. Furthermore, the results indicate that load-following with the MED process is more challenging than with RO.

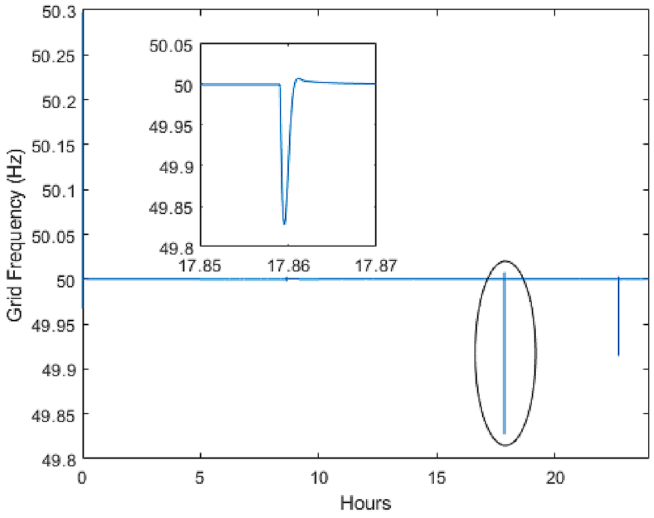

Fig. 16. HS1 (winter): Grid frequency during the reactor load follow with battery pack.

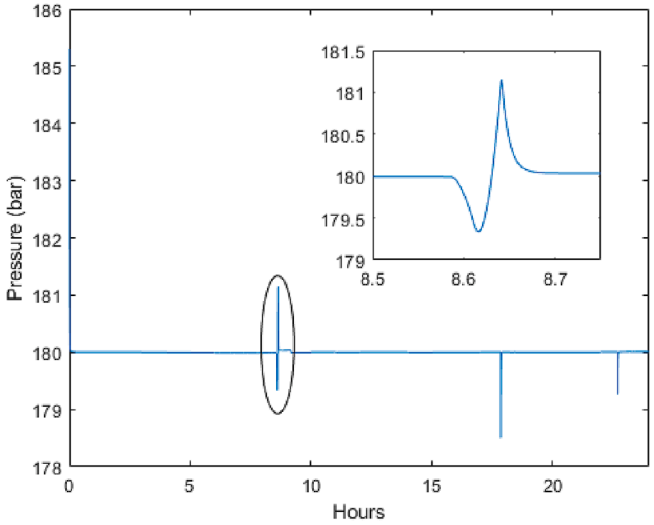

Fig. 17. HS1 (winter): Plant pressure.

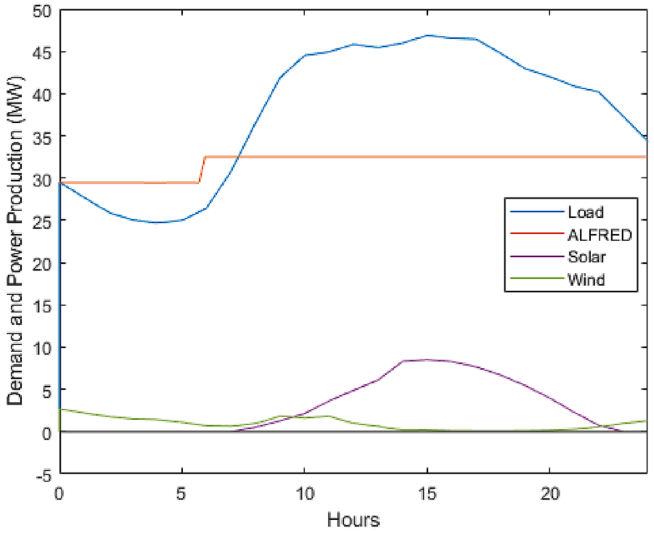

Fig. 18. HS2: Electrical demand and contributions.

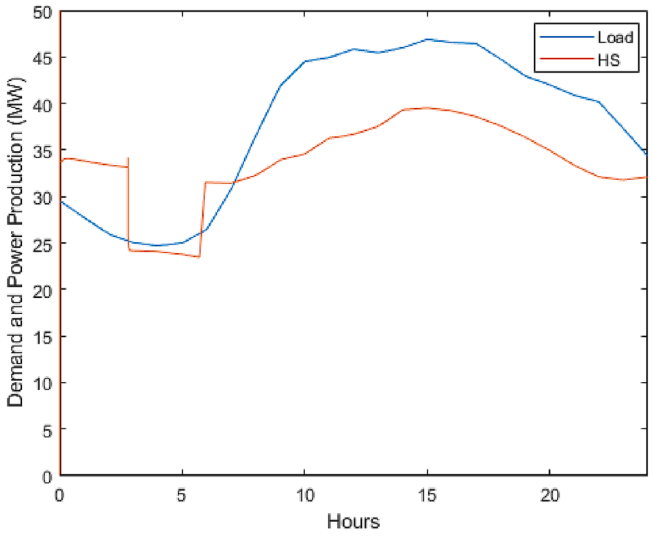

Fig. 19. HS2: Electrical demand VS. Total power produced.

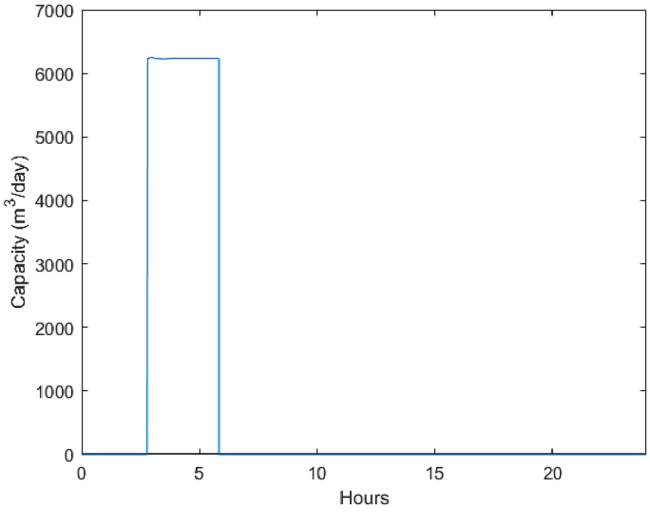

Fig. 20. MED electrical and thermal power absorbed from GENIV-SMR.

5. Conclusions

This study found that integrating an RO desalination plant into the hybrid system is more efficient and straightforward compared to integrating an MED desalination plant. The use of steam from the SMR for thermal utilization posed technical challenges, such as the need for turbine modifications to enable steam extraction and a more complex control strategy. The integration of desalination capacity into the system allowed for the calculation of the total daily water production for each scenario, as summarized in Table 6.

The primary metric used for comparing and evaluating the four case studies is the deviation of the electrical power generated by the hybrid system from the power demand requested by the grid. This deviation, which could be positive or negative, represents the impact of the local hybrid system on the grid stability, as shown in Fig. 21. The inclusion of

Table 6
Total fresh water produced in the various scenarios.

Scenario	Water production (m^3)
HS1 (summer), RO	$4.1 \cdot 10^3$
HS2, MED	$1.51 \cdot 10^3$

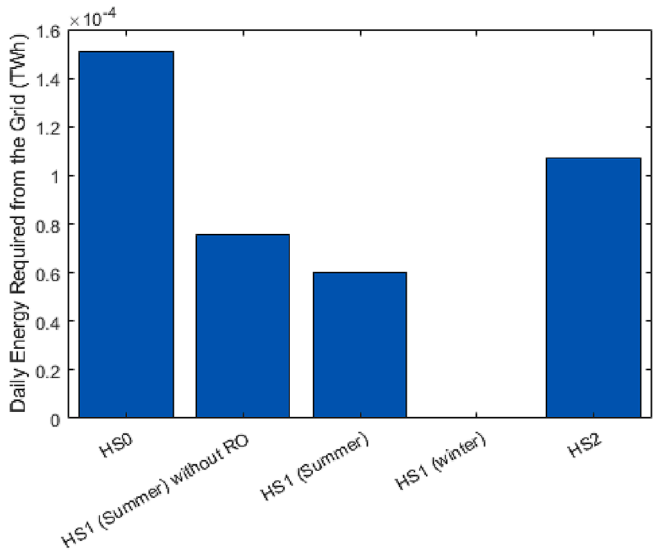

Fig. 21. Electrical energy taken from and sent to the grid to compensate the demand.

a case without RO is done to demonstrate the enhancement that cogeneration provides to case HS1. This metric provides a quantitative measure of how well the hybrid system aligns with the grid demand and helps assess the performance and effectiveness of the system in meeting the desired power output while maintaining grid stability.

As a preliminary study, the results indicate that the implementation of battery storage and RO desalination technology in a hybrid system can effectively reduce stress on the external grid when the reactor is operating in a load-following configuration. This approach provides a reliable source of fresh water while meeting power demands. However, operating in load-following mode may result in a reduced capacity factor, and integrating battery storage may increase operational and maintenance challenges, leading to increased O&M costs, if not properly accounted for. It is important to note that the timeframe of the simulations in this study is not on a yearly basis, and further work needs to be done to evaluate system performance over longer timeframes. Overall, the results highlight the potential of hybrid systems to balance energy demands and provide sustainable secondary goods (such as freshwater production), but more in-depth research is needed to fully understand the economic feasibility and optimal configuration of such systems under specific boundary conditions. This research opens up possibilities for future energy and water production studies, and further exploration and analysis are recommended to fully realize the potential of this technology in meeting our growing needs.

CRediT authorship contribution statement

Riccardo Chebac: Conceptualization, Methodology, Software, Visualization, Writing – original draft, Writing – review & editing. **Antonio Cammi:** Validation, Writing – review & editing. **Marco E. Ricotti:** Validation, Writing – review & editing. **Stefano Lorenzi:** Validation, Writing – review & editing. **Khashayar Sadeghi:** Methodology, Software, Writing – review & editing. **Seyed Hadi Ghazaie:** Methodology, Software, Writing – review & editing. **Ekaterina Sokolova:** Validation, Writing – review & editing. **Evgeniy Fedorovich:** Validation, Writing – review & editing.

Declaration of Competing Interest

The authors declare that they have no known competing financial interests or personal relationships that could have appeared to influence the work reported in this paper.

Data availability

Data will be made available on request.

Appendix A. Reactor controller tuning

The controller is tuned in such a way to obtain the desired droop value which is defined as:

$$\sigma = -100\frac{\Delta f/f_0}{\Delta P/P_0} \tag{14}$$

with f_0 and P_0 are the nominal frequency of the grid (50 Hz) and the nominal power of the reactor (130 MWe) respectively. The droop value σ has to be kept in the range 4–5.7% for NPPs (Sterpu, 2009; Kerlin and Upadhyaya, 2019). Thus, the general form of the controller can now be calculated as:

$$R(s) = \frac{1}{\sigma}(1+s\tau)\left(\frac{1}{1+sT_a}\right) \tag{15}$$

with the second term being the dynamics of the actuator with T_a being its characteristic time constant and is equal to $T_a = 0.2$–$0.4\ s$ and $\tau = 0.4\ s$. This approach is sufficient to guarantee stabilization to a new steady state in case of external perturbations. Table 7 shows the connection between each control variable with its controlled variable and what type of loop is used and Fig. 22 provides a schematic of the entire control loop.

Table 7
Pairings between input and output variables for the control strategy.

Control variable	Controlled variable	Loop
Control rods height	Thermal power	Feedback
Bypass valve	SG pressure	Feedback
Turbine admission valve	Mechanical power	Feedback + Feedforward
Feedwater mass flow rate	Cold leg temperature	Feedback + Feedforward
Turbine low-pressure valve	Cogeneration thermal power	Feedback

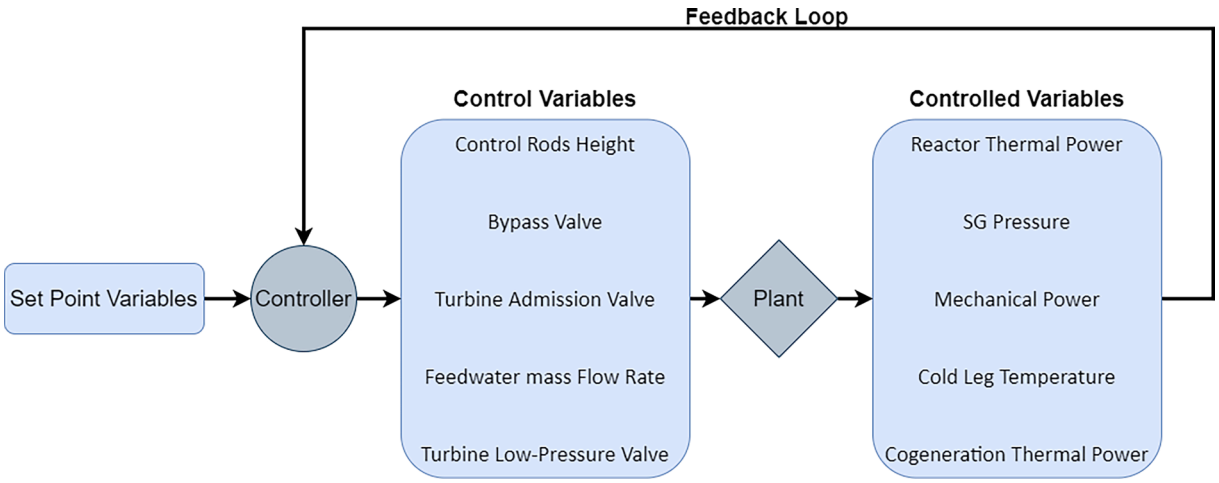

Fig. 22. ALFRED power plant controller scheme.

Appendix B. Desalination plant modeling

Detailed information on the modeling of the thermal and membrane DPs is reported elsewhere (Kavvadias and Khamis, 2010; Sadeghi et al., 2020). Briefly, the maximum water capacity (in m^3/day), which can be produced by a certain amount of heat is given by:

$$Thermal\ Capacity = \frac{(GOR{\cdot}24{\cdot}3600)}{\Delta H_{Tim}} \tag{16}$$

where Tim is the intermediate loop temperature and GOR is the gain output ratio of the thermal DP and can be obtained by:

$$GOR(MED) = 0.7{\cdot}\frac{(MBT - TLS)}{ATD} \tag{17}$$

$$GOR(MSF) = \frac{\Delta H_{Tim}}{CH(T_{ih} + T_{be})}\left(1 - exp\frac{(cvmT_{ov})}{\Delta H_{\frac{MBT+TLS}{2}}}\right) \tag{18}$$

Where MBT and TLS are the Maximum Brine Temperature (°C) and Temperature of the Last Effect (°C), respectively, ATD is the Average Temperature Difference between the effects (°C), CH is the specific heat capacity of the water in the brine heater(kj/ kg· K), T_{ih} is the temperature of heated water after the brine heater (°C), T_{be} is average boiling point elevation, cvm is the average specific heat of the brine, (kj/kg·K) and T_{ov} is the average operating temperature of MSF plant (°C).

$$RO\ capacity\left[\frac{m^3}{day}\right] = \frac{Input\ Power\ [MW]}{A_1 + A_2 + A_3} \tag{19}$$

With:

$$A_1 = \frac{1000}{24{\cdot}3600{\cdot}Recovery\ ratio\ of\ RO\ unit} \tag{20}$$

$$A_2 = \left(\frac{DPhm{\cdot}Eem{\cdot}kmSGW}{Ehm{\cdot}Ehhm{\cdot}9866}\right) + \left(\frac{DPsm}{Esm} + \frac{DPbm}{Ebm}\right)\left(\frac{Eem{\cdot}kmSGW}{9866}\right) - (1 - \text{ Recovery ratio }) \left(\frac{DPhm{\cdot}Eer{\cdot}kmSGW}{Ehm{\cdot}Ehhm{\cdot}9866}\right) \tag{21}$$

$$A_3 = \frac{Q_{OS}}{24{\cdot}1000} \tag{22}$$

where DPhm is the high head pump pressure rise (bar), Eem the high head pump power (MW), kmSGW is the specific gravity of seawater feed correction factor, Ehm is the high head pump efficiency, Ehhm is hydraulic pump hydraulic coupling efficiency, Esm is Seawater pump efficiency, Ebm is booster pump efficiency, DPsm is seawater pump head (bar), DPbm is the booster pump head (bar) and Q_{OS} is other specific power used in RO unit (MW).

References

Federico Agosti, Lelio Luzzi, et al. Heat transfer correlations for liquid metal cooled fast reactors, 2007.

Akcasuh, Z., 2012. Mathematical methods in nuclear reactor dynamics. Elsevier.

Alessandro Alemberti, M Frogheri, Luigi Mansani, et al. The lead fast reactor: demonstrator (alfred) and elfr design. 2013.

Al-Karaghouli, A., Kazmerski, L., 2013. Energy consumption and water production cost of conven- tional and renewable-energy-powered desalination processes. Renew. Sustain. Energy Rev. 24, 343–356.

Arroyo M, F.R., Miguel, L.J., 2020. The role of renewable energies for the sustainable energy governance and environmental policies for the mitigation of climate change in Ecuador. Energies 13 (15), 3883.
Ayamolowo, O.J., Manditereza, P.T., Kusakana, K., 2020. Exploring the gaps in renewable energy integration to grid. Energy Rep. 6, 992–999.
Casella, F., Leva, A., 2005. Object-oriented modelling & simulation of power plants with modelica. In: Proceedings of the 44th IEEE Conference on Decision and Control, pp. 7597–7602.
Charge/discharge control of battery energy storage system for peak shaving yahia baghzouz. https://www.sandia.gov/ess-ssl/EESAT/2009_papers/Charge%20-%20Discharge%20Control%20of%20Battery%20Energy%20Storage%20System%20for%20Peak%20Shaving.pdf.
R Chebac, A Cammi, ME Ricotti, K Sadeghi, SH Ghazaie, E Sokolova, E Fedorovich, et al. Dynamic response of lfr in cogeneration mode. In *Proceedings of the International Conference Nuclear Energy for New Europe (NENE 2021)*, number 204, pages 1–8. SVN, 2021.
Dag Brück, Hilding Elmqvist, Sven Erik Mattsson, and Hans Olsson. Dymola for multi-engineering modeling and simulation. In *Proceedings of modelica*, volume 2002. Citeseer, 2002.
Dimensioning of current transformers for protection applications. https://store.gegridsolutions.com/faq/Documents/General/GER-3973A.pdf.
Dizqah, A.M., Maheri, A., Busawon, K., Fritzson, P., 2013. Acausal modelling and dynamic simulation of the standalone wind-solar plant using modelica. In: 2013 UKSim 15th International Conference on Computer Modelling and Simulation. IEEE, pp. 580–585.
Dong, Z., Pan, Y., Zhang, Z., Dong, Y., Huang, X., 2018. Dynamical modeling and simulation of the six-modular high temperature gas-cooled reactor plant htr-pm600. Energy 155, 971–991.
Dong, Z., Liu, M., Huang, X., Zhang, Y., Zhang, Z., Dong, Y., 2019. Dynamical modeling and simulation analysis of a nuclear desalination plant based on the med-tvc process. Desalination 456, 121–135.
Dong, Z., Pan, Y., 2018. A lumped-parameter dynamical model of a nuclear heating reactor cogeneration plant. Energy 145, 638–656.
Elmqvist, H., Mattsson, S.E., Otter, M., 1998. Modelica: The new object-oriented modeling language. In *12th European Simulation Multiconference* volume 5.
Konor L. Frick, Paul W. Talbot, Daniel S. Wendt, Richard D. Boardman, Cristian Rabiti, Shan- non M. Bragg-Sitton, Mark Ruth, Daniel Levie, Bethany Frew, Amgad Elgowainy, and Troy Hawkins. Evaluation of hydrogen production feasibility for a light water reactor in the midwest. 9 2019.
Konor L Frick, Shannon M Bragg-Sitton, and Cristian Rabiti. Development of the inl thermal energy distribution system (teds) in the modelica eco-system for validation and verification. Tech- nical report, Idaho National Lab.(INL), Idaho Falls, ID (United States), 2020.
Ghazaie, S.H., Sadeghi, K., Sokolova, E., Fedorovich, E., Shirani, A., Vatin, N., Zunino, P., Vdovin, E., 2019. Nuclear desalination in Iran, current status and perspectives. E3S Web Conf. 140, 04001.
Ghazaie, S.H., Sadeghi, K., Sokolova, E., Fedorovich, E., Shirani, A., 2020. Comparative Analysis of Hybrid Desalination Technologies Powered by SMR. Energies 13 (19), 5006.
DT Ingersoll, C Colbert, Z Houghton, R Snuggerud, JW Gaston, and M Empey. Can nuclear power and renewables be friends? In *Proceedings of ICAPP*, volume 9, 2015.
International Atomic Energy Agency. Opportunities for cogeneration with nuclear energy. *NP- T-4.1*, 2017.
Jerome Serp, Michel Allibert, Ondřej Benes̆, Sylvie Delpech, Olga Feynberg, Véronique Ghetta, Daniel Heuer, David Holcomb, Victor Ignatiev, Jan Leen Kloosterman, et al. The molten salt reactor (msr) in generation iv: overview and perspectives. *Progress in Nuclear Energy*, 77:308–319, 2014.
Jonathan LeSage. Microgrid system development and analysis. https://www.mathworks.com/videos/series/microgrid-system-development-and-analysis.html.
Kavvadias, K.C., Khamis, I., 2010. The iaea deep desalination economic model: a critical review. Desalination 257 (1–3), 150–157.
Kerlin, T.W., Upadhyaya, B.R., 2019. Dynamics and control of nuclear reactors. Academic press.
Kh Ibragimov, M., Subbotin, V.I., Ushakov, P.A., 1961. Investigation of heat transfer in the turbulent flow of liquid metals in tubes. The Soviet Journal of Atomic Energy 8 (1), 48–50.
Kober, T., Schiffer, H.-W., Densing, M., Panos, E., 2020. Global energy perspectives to 2060–wec's world energy scenarios 2019. Energy Strat. Rev. 31, 100523.
Krautmann, A.C., Solow, J.L., 1988. Economies of scale in nuclear power generation. South. Econ. J. 55 (1), 70.
Lee, W.-J., Kim, Y.-W., Chang, J.-H., 2009. Perspectives of nuclear heat and hydrogen. Nucl. Eng. Technol. 41 (4), 413–426.
Locatelli, G., Fiordaliso, A., Boarin, S., Ricotti, M.E., 2017. Cogeneration: An option to facilitate load following in small modular reactors. Prog. Nucl. Energy 97, 153–161.
Giorgio Locatelli. Why are megaprojects, including nuclear power plants, delivered overbudget and late? reasons and remedies. *arXiv preprint arXiv:1802.07312*, 2018.
Lokhov, Alexey, 2011. Technical and economic aspects of load following with nuclear power plants. NEA, OECD, Paris, France.
Daniel Mark Mikkelson, Konor L Frick, Cristian Rabiti, and Shannon M Bragg-Sitton. Ther- mal energy storage model development within the integrated energy systems hybrid repository. Technical report, Idaho National Lab.(INL), Idaho Falls, ID (United States), 2021.
New Technologies for Seawater Desalination Using Nuclear Energy. Number 1753 in TECDOC Series. INTERNATIONAL ATOMIC ENERGY AGENCY, Vienna, 2015.
Nuclear–renewable hybrid energy systems for decarbonized energy production and cogeneration. https://www-pub.iaea.org/MTCD/Publications/PDF/TE-1885web.pdf.
OECD Nuclear Energy Agency, 2021. Technical and economic aspects of load following with nuclear power plants. Technical report. OECD Nuclear Energy Agency.
Oka, Y., Suzuki, K., et al., 2013. Nuclear Reactor Kinetics and Plant Control, 10. Springer.
Opportunities for Cogeneration with Nuclear Energy. Number NP-T-4.1 in Nuclear Energy Series. INTERNATIONAL ATOMIC ENERGY AGENCY, Vienna, 2017.
Otter, M., Elmqvist, H., Cellier, Francois E., 1996. Modeling of multibody systems with the object-oriented modeling language dymola. Nonlinear Dyn. 9, 91–112.
Ponciroli, R., Bigoni, A., Cammi, A., Lorenzi, S., Luzzi, L., 2014. Object- oriented modelling and simulation for the alfred dynamics. Prog. Nucl. Energy 71, 15–29.
Ponciroli, R., Cammi, A., Lorenzi, S., Luzzi, L., 2015. Control approach to the load frequency regulation of a generation iv lead-cooled fast reactor. Energ. Conver. Manage. 103, 43–56.
Magdi Ragheb and Adam M Ragheb. Wind turbines theory-the betz equation and optimal rotor tip speed ratio. *Fundamental and advanced topics in wind power*, 1(1):19–38, 2011.
Sadeghi, K., Ghazaie, S.H., Sokolova, E., Fedorovich, E., Shirani, A., 2020. Evgeniy Fedorovich, and Amirsaeed Shirani. Comprehensive techno-economic analysis of integrated nuclear power plant equipped with various hybrid desalination systems. Desalination 493, 114623.
Son, I.W., Jeong, Y.H., Choi, Y.J., Lee, J.I., 2021. Feasibility study of solar-nuclear hybrid system for distributed power source. Energ. Conver. Manage. 230, 113808.
Sterpu, S., 2009. Power system dynamic performance: Primary governing frequency response. In: In *2009 IEEE Bucharest PowerTech*. IEEE, pp. 1–6.
Hadid Subki. Advances in small modular reactor technology developments. 2020.
Suman, S., 2018. Hybrid nuclear-renewable energy systems: A review. J. Clean. Prod. 181, 166–177.
Wang, G., Yin, J., Lin, J., Chen, Z., Hu, P., 2021. Design and economic analysis of a novel hybrid nuclear-solar complementary power system for power generation and desalination. Appl. Therm. Eng. 187, 116564.
https://it.weatherspark.com.
Yap, K.Y., Sarimuthu, C.R., Lim, J.-Y., 2019. Virtual inertia-based inverters for mitigating frequency instability in grid-connected renewable energy system: A review. Appl. Sci. 9 (24), 5300.
You, H., Simner, S.P., Wagner, R.M., Phillips, J., Terpstra, T., Kupitz, B., Hartvigsen, J.J., Cetiner, S.M., 2017. Status report on the high-temperature steam electrolysis plant model developed in the modelica framework (fy17). Idaho National Laboratory (INL). Technical report,.
Youssef, P.G., Al-Dadah, R.K., Mahmoud, S.M., 2014. Comparative analysis of desalination technologies. Energy Procedia 61, 2604–2607.
Zohuri, B., 2020. Generation iv nuclear reactors. In: Nuclear Reactor Technology Development and Utilization. Elsevier, pp. 213–246.